

36. L. Landau, E. Lifshitz, *Fluid Mechanics*, vol. 225 (Pergamon, New York, 1959).
37. D. Ruelle, F. Takens, *Commun. Math. Phys.* **20**, 167 (1971).
38. H. Chaté, P. Manneville, *Physica D* **32**, 409 (1988).
39. J. Rolf, T. Bohr, M. Jensen, *Phys. Rev. E Stat. Phys. Plasmas Fluids Relat. Interdiscip. Topics* **57**, R2503 (1998).
40. L. D. Brown, T. T. Cai, A. DasGupta, *Stat. Sci.* **16**, 101 (2001).

Acknowledgments: We thank A. P. Willis for sharing his hybrid spectral finite-difference code. We acknowledge the Deutsche Forschungsgemeinschaft (project FOR 1182), the Max Planck Society, and the Engineering and Physical Sciences Research Council (grant EP/F017413/2) for

financial support. D.B. thanks the Leverhulme Trust and the Royal Society for their support. M.A. and B.H. acknowledge computing resources from GWDG (Gesellschaft für wissenschaftliche Datenverarbeitung Göttingen) and the Jülich Supercomputing Centre (grant HGU16), where DNS2 were performed. D.M. and D.B. acknowledge computing resources from the Centre for Scientific Computing, University of Warwick, and Grand Equipement National de Calcul Intensif-Institut du Développement et des Ressources en Informatique Scientifique (grants 2010-1119 and 2011-1119), where DNS1 were performed. K.A. acknowledges support from the International Max

Planck Research School for the Physics of Biological and Complex Systems and the Göttinger Graduate School for Neurosciences and Molecular Biosciences.

Supporting Online Material

www.sciencemag.org/cgi/content/full/333/6039/192/DC1
Materials and Methods
Figs. S1 to S5
Tables S1 to S3
References

24 January 2011; accepted 19 May 2011
10.1126/science.1203223

REPORTS

Frequency Metrology in Quantum Degenerate Helium: Direct Measurement of the $2^3S_1 \rightarrow 2^1S_0$ Transition

R. van Rooij,¹ J. S. Borbely,¹ J. Simonet,² M. D. Hoogerland,³ K. S. E. Eikema,¹
R. A. Rozendaal,¹ W. Vassen^{1*}

Precision spectroscopy of simple atomic systems has refined our understanding of the fundamental laws of quantum physics. In particular, helium spectroscopy has played a crucial role in describing two-electron interactions, determining the fine-structure constant and extracting the size of the helium nucleus. Here we present a measurement of the doubly forbidden 1557-nanometer transition connecting the two metastable states of helium (the lowest energy triplet state 2^3S_1 and first excited singlet state 2^1S_0), for which quantum electrodynamic and nuclear size effects are very strong. This transition is weaker by 14 orders of magnitude than the most predominantly measured transition in helium. Ultracold, submicrokelvin, fermionic ^3He and bosonic ^4He atoms are used to obtain a precision of 8×10^{-12} , providing a stringent test of two-electron quantum electrodynamic theory and of nuclear few-body theory.

The first observations of helium emission spectra at the end of the 19th century revealed two separate series of lines, associated with orthohelium and parahelium, respectively. In 1926, Heisenberg explained the distinction between these two spectra on the basis of wave mechanics, electron spin, and the Pauli exclusion principle (1). The spectrum of orthohelium arises from triplet states for which the electron spins are parallel, whereas in parahelium the electron spins are antiparallel, forming singlet states (Fig. 1). From the lowest state of orthohelium, the $1s2s^3S_1$ state (denoted 2^3S_1), only excitations to triplet states have been observed. Orthohelium transitions from the 2^3S_1 state and associated studies of the $n^3P_{0,1,2}$ ($n = 2,3$) fine-structure splittings (2–7) have enabled tests of quantum electrodynamics (QED) (8, 9), as well as a determination of the fine-structure constant (5, 10). In the singlet spectrum of helium (parahelium), electric-dipole

transitions from the 1^1S_0 ground state (11) and from the metastable 2^1S_0 state (12, 13) have also provided tests of high-precision QED calculations. All these frequency metrology studies have been performed using either atomic beams or gas discharges. However, helium in the metastable 2^3S_1 state (He^* , lifetime 8×10^3 s) can be laser-cooled and trapped, which allows much longer interaction times for excitation of weak transitions. He^* atoms have been cooled to μK temperatures,

which revealed quantum statistical effects of bunching and antibunching (14) and allowed quantum degeneracy to be achieved for both the bosonic isotope ^4He (15, 16) and the fermionic isotope ^3He (17).

Here we observe an orthohelium-parahelium transition, specifically, the 1557-nm transition between the metastable 2^3S_1 and 2^1S_0 states (Fig. 1), both in ^4He and ^3He . This transition is an excellent testing ground for fundamental theory of atomic structure. Because of a large electron density at the nucleus, the energy of S states is the most sensitive to QED and to nuclear size effects (8). For the 2^3S_1 and 2^1S_0 metastable states, QED terms contribute 4 and 3 GHz respectively, to a total binding energy of 10^6 GHz (8, 9). The present accuracy in the QED calculations is 2 MHz, based on an estimate of non-evaluated higher-order terms. Many of these terms are common between the isotopes. Therefore, in the calculation of the isotope shift (i.e., the difference between the transition frequencies for ^4He and ^3He), mass-independent terms cancel, and the uncertainty is reduced to the sub-kHz level (18). As the finite nuclear charge radius shifts the 2^3S_1 state by 2.6 MHz and the 2^1S_0 state by 2.0 MHz, an accurate isotope-shift measurement allows a sensitive determination of the difference in the mean charge radius of the α particle and of the ^3He nucleus, which provides a stringent test of nuclear charge radius calculations and experiments (19).

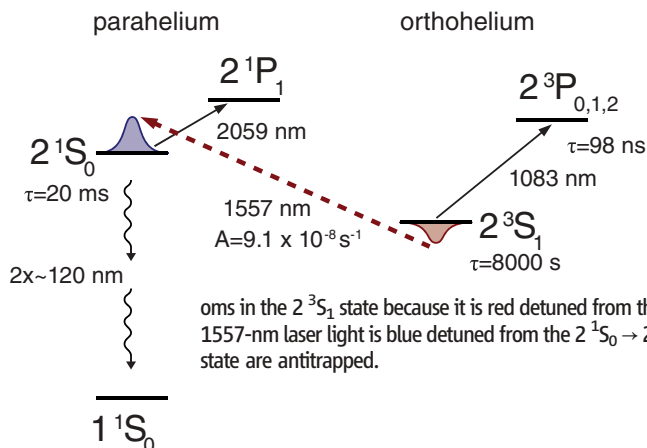


Fig. 1. Relevant energy levels, transition wavelengths, and state lifetimes of helium. The magnetic-dipole transition connecting the 2^3S_1 state and the 2^1S_0 state has a wavelength of 1557 nm and an Einstein A coefficient of $9.1 \times 10^{-8} \text{ s}^{-1}$. A focused 1557-nm laser also constitutes a trap for ultracold atoms in the 2^3S_1 state because it is red detuned from the $2^3S_1 \rightarrow 2^3P_1$ transitions. As the 1557-nm laser light is blue detuned from the $2^1S_0 \rightarrow 2^1P_1$ transition, atoms in the 2^1S_0 state are antitrapped.

¹LaserLab Vrije Universiteit, De Boelelaan 1081, 1081 HV Amsterdam, Netherlands. ²Ecole Normale Supérieure, Laboratoire Kastler-Brossel, 24 rue Lhomond, 75005 Paris, France. ³Department of Physics, University of Auckland, Private Bag 92019, Auckland, New Zealand.

*To whom correspondence should be addressed. E-mail: w.vassen@vu.nl

The natural linewidth of the $2^3S_1 \rightarrow 2^1S_0$ transition is 8 Hz, determined by the 20-ms lifetime of the 2^1S_0 state, which relaxes via two-photon decay to the ground state (Fig. 1). This transition is 200,000 times as narrow as the natural linewidth of the 2^3P state, which is most prominently used for spectroscopy in helium. The Einstein A coefficient for the $2^3S_1 \rightarrow 2^1S_0$ magnetic-dipole transition is $\sim 10^{-7} \text{ s}^{-1}$ (20, 21), smaller by 14 orders of magnitude than for the electric-dipole transitions from 2^3S_1 to $2^3P_{0,1,2}$ states, which indicates that excitation requires high power and/or long interaction times.

The experiment described here was performed using an apparatus designed for the production of quantum degenerate gases of helium (17, 22). Briefly, the metastable 2^3S_1 state is populated

by electron impact in an electric discharge. The atomic beam is collimated, slowed, and trapped by using standard laser cooling and trapping techniques on the $2^3S_1 \rightarrow 2^3P_2$ transition at 1083 nm. The atoms, optically pumped to $m_J = +1$, are then transferred to an Ioffe-Pritchard-type magnetic trap. $^4\text{He}^*$ atoms are evaporatively cooled toward Bose-Einstein condensation by stimulating radio-frequency (RF) transitions to untrapped states. For $^3\text{He}^*$ (in the $F = 3/2$ hyperfine state), quantum degeneracy is reached by sympathetic cooling with $^4\text{He}^*$. Either one or both of the two isotopes are transferred into a crossed-beam optical dipole trap. This trap consists of two focused 1557-nm laser beams, intersecting at their foci, as shown in Fig. 2. We transfer up to 10^6 atoms to this optical trap.

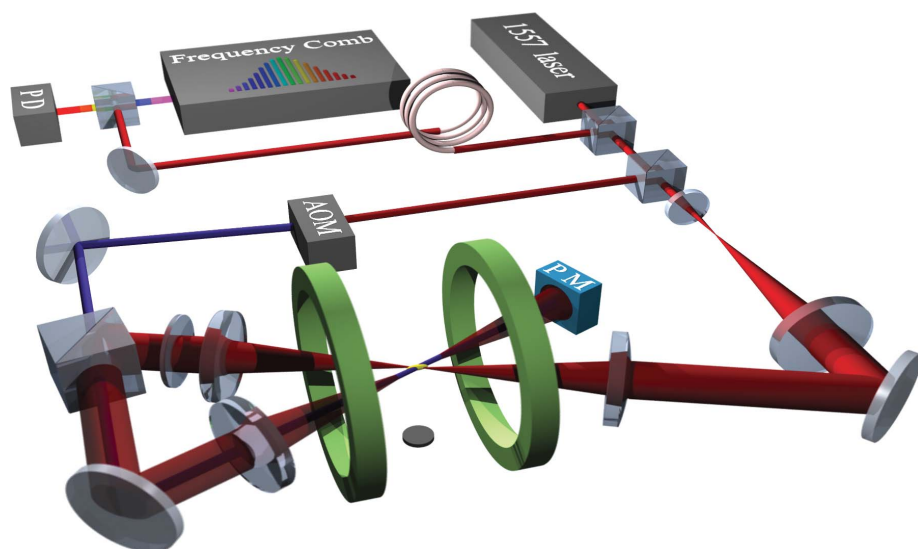


Fig. 2. Experimental setup. A small fraction of the 1557-nm laser light is split off and coupled via a fiber-optic link to be referenced to a fiber-based frequency comb. A heterodyne signal is monitored on a fast photodiode (PD) to determine the absolute frequency of the 1557-nm laser. The remaining light is divided into the trap beam and the spectroscopy beam. A crossed-beam dipole trap configuration is realized by focusing both the incident and returning trap beam (with orthogonal linear polarizations) to a waist of $\sim 85 \mu\text{m}$ at the center of the magnetic trap (represented by the green coils) under a relative angle of 19 degrees, trapping atoms at the intersection. The spectroscopy beam is frequency shifted by a 40-MHz acousto-optical modulator (AOM), overlapped with the returning trap beam and absorbed by a thermopile power meter (PM). A microchannel plate detector is positioned underneath the trap for temperature and atom number determination.

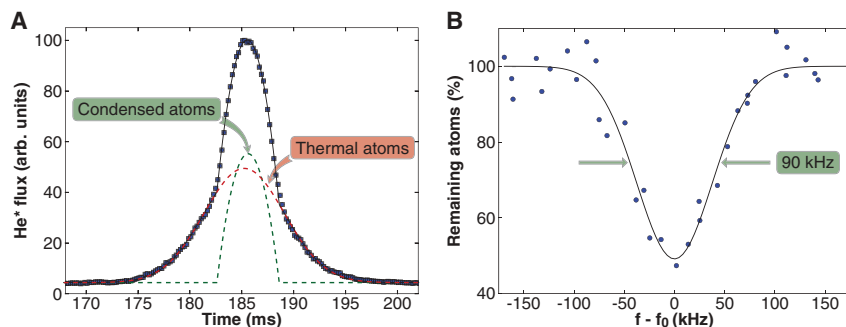


Fig. 3. (A) Bimodal time-of-flight distribution observed when He^* atoms are detected on the MCP detector ~ 186 ms after the trapping laser light is turned off. The MCP signal is fit to determine the number of Bose-condensed atoms. (B) The percentage of Bose-condensed ^4He atoms remaining in the 2^3S_1 state as a function of applied laser frequency (relative to the fitted center frequency f_0). The line is a fit of a Gaussian to the data. We measure linewidths varying from 75 to 130 kHz depending on the trap depth and on the isotope.

After loading the optical trap, the atoms are illuminated by a separate beam for spectroscopy, which is derived from the same laser as the optical trap beam, but is switched and frequency-shifted by a 40-MHz acousto-optic modulator. A heterodyne signal is set up between the 1557-nm laser and a mode of a femtosecond frequency-comb laser to deduce the absolute frequency of the spectroscopy laser. The frequency comb is based on a mode-locked erbium-doped fiber laser, for which both the repetition rate and the carrier-envelope offset frequency are referenced to a global positioning system-controlled Rubidium clock (23).

After a certain interaction time (typically 1 to 6 s), both the spectroscopy beam and the trap beam are switched off, which allows the atoms to fall because of gravity. The high internal energy of He^* (20 eV above the 1^1S_0 ground state) allows for efficient detection on a microchannel plate (MCP) detector (Fig. 2). The MCP signal reflects both the number of atoms and their temperature. In the case of ^4He , the signal has a bimodal character that results from the combination of Bose-condensed atoms and thermal atoms (Fig. 3A); a fit to this signal provides the number of condensed atoms (23). Because the excited state is antitrapped, the trap is depleted when the spectroscopy beam is resonant with the atomic transition. By deducing the remaining number of 2^3S_1 atoms for various laser frequencies, the atomic resonance frequency is determined from a Gaussian fit to the data (Fig. 3B). The observed linewidth is largely due to the 75-kHz laser linewidth.

Several systematic shifts in the transition frequency are taken into account (23). The largest shift is due to the Zeeman effect. The measured transition, $2^3S_1 (m_J = +1) \rightarrow 2^1S_0 (m_J = 0)$ for ^4He , and $2^3S_1, F = 3/2 (m_F = +3/2) \rightarrow 2^1S_0, F = 1/2 (m_F = +1/2)$ for ^3He , is shifted from resonance predominantly by Earth's magnetic field. The size of the shift is deduced by measuring the resonance frequency of RF spin-flip transitions between the 2^3S_1 magnetic substates. An additional shift is caused by the momentum transfer from a 1557-nm photon to an atom. In the case of ^4He , the high density of the condensate could potentially cause a mean-field shift (24). However, by performing the experiment with reduced atomic density, no shift is observed.

The second-largest systematic frequency perturbation is due to the AC Stark shift associated with the intense 1557-nm light that induces the dipole trap: The specific energy state of the trapping potential for an atom determines the AC Stark shift for that atom. For ^4He , only excitations of atoms condensed in the ground state of the dipole trap are taken into account in determining the transition frequency. As the trap depth depends linearly on laser intensity, measuring the resonance frequency for a range of applied laser powers allows an extrapolation to zero laser intensity. In contrast, ^3He atoms, because of their fermionic nature, are distributed throughout the energy states of the dipole trap, and as a result,

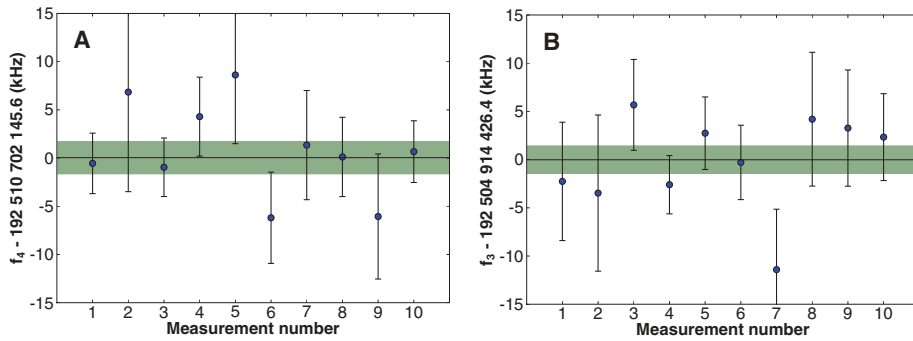


Fig. 4. Measured transition frequencies for ${}^4\text{He}$ (A) and for ${}^3\text{He}$ (B). The error bar on each data point includes contributions from various systematic sources, e.g., AC Stark shift and Zeeman shift (23). The frequencies quoted on the y axes are the weighted averages of the data points. Their associated uncertainties (with the uncertainties due to the frequency comb calibration and the mean-field shift added in quadrature) are ± 1.8 kHz for ${}^4\text{He}$ and ± 1.5 kHz for ${}^3\text{He}$, represented by the green bands.

the measured AC Stark shift does not equal the trap depth (as is the case with ${}^4\text{He}$) but is reduced due to the density of states within the dipole trap. A nonlinear shift can then potentially arise at high laser intensities, where the larger trap depths allow for higher temperatures. To minimize this effect, ${}^3\text{He}$ atoms are sympathetically cooled to the quantum degenerate regime to populate predominantly the lowest energy states of the trapping potential. Over the course of several months, 20 independent extrapolations were obtained (as shown in Fig. 4) to deduce an absolute frequency of the $2\ {}^3\text{S}_1 \rightarrow 2\ {}^1\text{S}_0$ transition for ${}^4\text{He}$ of $f_4 = 192,510,702,145.6(1.8)$ kHz and for ${}^3\text{He}$ ($F = 3/2 \rightarrow F = 1/2$) of $f_3 = 192,504,914,426.4(1.5)$ kHz, where the one-standard deviation error in parentheses includes all statistical and systematic uncertainties.

For both isotopes, our result agrees with QED calculations of the ionization energies of the two metastable states (9, 25). The present experimental error in the transition frequency is smaller by three orders of magnitude than estimates of non-evaluated higher-order terms in state-of-the-art QED calculations and presents a significant challenge for groups involved in atomic structure theory.

An indirect value of the energy difference between the $2\ {}^3\text{S}_1$ and the $2\ {}^1\text{S}_0$ states can be obtained from the literature (only for ${}^4\text{He}$) by combining experimental transition frequencies from both metastable states to high-lying S, P, and D states with theoretical values for the ionization energies of these states. This procedure yields ionization energies for the $2\ {}^1\text{S}_0$ state (8, 12, 13) and the $2\ {}^3\text{S}_1$ state (2, 8), and the difference between these values gives a transition frequency of $192,510,701.96(16)$ MHz, in agreement with our result, although with much lower precision.

Isotope shift measurements, combined with high-precision QED theory, provide a method for isolating contributions due to finite nuclear size effects. The difference in nuclear charge radii between ${}^3\text{He}$ and ${}^4\text{He}$ is determined by comparing experiment and theory. The ${}^4\text{He}$ nuclear charge radius is one of the most precisely known of all nuclei (26), $1.681(4)$ fm. A value of the ${}^3\text{He}$ nu-

clear charge radius can then be deduced with similar precision. In calculating the isotope shift, QED theory is more precise than our measurement, as mass-independent terms cancel. The theoretical value for the isotope shift (if one assumes pointlike nuclei) is $8,034,148.6(7)$ kHz (23). Subtracting the measured transition frequencies and correcting for the accurately known hyperfine structure (f_{hfs}) (25, 27), we find an isotope shift of $f_4 - f_3 + f_{\text{hfs}} = 8,034,367.2(2.3)$ kHz. The 218.6-kHz difference may be attributed to the finite size of both nuclei. This nuclear shift is proportional to the difference in the nuclear charge radii squared, $\Delta r_c^2 \equiv r_c^2({}^3\text{He}) - r_c^2({}^4\text{He})$. Using the theoretical proportionality constant of 4.6642 fm²/MHz (18) for the measured transition, we deduce $\Delta r_c^2 = 1.019(11)$ fm². Δr_c^2 represents a more universal parameter than the value of the isotope shift, as it is obtained from various branches of physics. Besides getting it through spectroscopic means, it can be determined from nuclear theory and from electron-scattering experiments. Nuclear few-body theory provides $\Delta r_c^2 = 1.16(12)$ fm² (18, 23, 28), whereas from electron-scattering experiments $\Delta r_c^2 = 1.01(13)$ fm² (26, 29). Comparing the values of Δr_c^2 , we find our result to be in good agreement but more precise by an order of magnitude. An independent spectroscopic measurement in helium on the $2\ {}^3\text{S}_1 \rightarrow 2\ {}^3\text{P}_0$ transition (30) gives $\Delta r_c^2 = 1.059(3)$ fm², obtained by using the most recent QED calculations (19). Although the measurement precision of the isotope shift for this transition is comparable to our precision, the smaller uncertainty in Δr_c^2 is due to a larger sensitivity to differential nuclear charge effects. At present, the accuracy to which the ${}^4\text{He}$ charge radius is known sets a lower limit on the uncertainty of the ${}^3\text{He}$ charge radius determined from helium spectroscopy. Our measurement presents a value for the ${}^3\text{He}$ nuclear charge radius of $1.961(4)$ fm.

We have also demonstrated that all of the trapped atoms can be transferred to the $2\ {}^1\text{S}_0$ state to produce a source of ultracold singlet helium. Optically trapping these atoms simultaneously with cold $1\ {}^1\text{S}_0$ ground-state atoms (produced

after two-photon decay) opens up the possibility of performing two-photon spectroscopy on the $2\ {}^1\text{S}_0 \leftrightarrow 1\ {}^1\text{S}_0$ transition (11, 31), where QED and nuclear size effects are strongest.

References and Notes

- W. Heisenberg, *Z. Phys.* **39**, 499 (1926).
- C. Dorrer, F. Nez, B. de Beauvoir, L. Julien, F. Biraben, *Phys. Rev. Lett.* **78**, 3658 (1997).
- P. C. Pastor *et al.*, *Phys. Rev. Lett.* **92**, 023001 (2004).
- P. Mueller *et al.*, *Phys. Rev. Lett.* **94**, 133001 (2005).
- M. Smiciklas, D. Shiner, *Phys. Rev. Lett.* **105**, 123001 (2010).
- J. S. Borbely *et al.*, *Phys. Rev. A* **79**, 060503 (2009).
- T. Zelevinsky, D. Farkas, G. Gabrielse, *Phys. Rev. Lett.* **95**, 203001 (2005).
- G. W. F. Drake, Z.-C. Yan, *Can. J. Phys.* **86**, 45 (2008).
- V. A. Yerokhin, K. Pachucki, *Phys. Rev. A* **81**, 022507 (2010).
- K. Pachucki, V. A. Yerokhin, *Phys. Rev. Lett.* **104**, 070403 (2010).
- D. Z. Kandalau, C. Gohle, T. J. Pinkert, W. Ubachs, K. S. Eikema, *Phys. Rev. Lett.* **105**, 063001 (2010).
- C. J. Sansonetti, J. D. Gillaspay, *Phys. Rev. A* **45**, R1 (1992).
- W. Lichten, D. Shiner, Z.-X. Zhou, *Phys. Rev. A* **43**, 1663 (1991).
- T. Jeltsov *et al.*, *Nature* **445**, 402 (2007).
- A. Robert *et al.*, *Science* **292**, 461 (2001).
- F. Pereira Dos Santos *et al.*, *Phys. Rev. Lett.* **86**, 3459 (2001).
- J. M. McNamara, T. Jeltsov, A. S. Tychkov, W. Hogervorst, W. Vassen, *Phys. Rev. Lett.* **97**, 080404 (2006).
- G. W. F. Drake, W. N. Mörtershäuser, Z.-C. Yan, *Can. J. Phys.* **83**, 311 (2005).
- D. C. Morton, Q. Wu, G. W. F. Drake, *Phys. Rev. A* **73**, 034502 (2006).
- G. Lach, K. Pachucki, *Phys. Rev. A* **64**, 042510 (2001).
- K. A. H. van Leeuwen, W. Vassen, *Europhys. Lett.* **76**, 409 (2006).
- A. S. Tychkov *et al.*, *Phys. Rev. A* **73**, 031603 (2006).
- Methods and calculations are further detailed in supporting material at Science Online.
- T. C. Killian *et al.*, *Phys. Rev. Lett.* **81**, 3807 (1998).
- D. C. Morton, Q. Wu, G. W. F. Drake, *Can. J. Phys.* **84**, 83 (2006).
- I. Sick, *Phys. Rev. C Nucl. Phys.* **77**, 041302 (2008).
- S. D. Rosner, F. M. Pipkin, *Phys. Rev. A* **1**, 571 (1970).
- A. Kievsky, S. Rosati, M. Viviani, L. E. Marcucci, L. Girlanda, *J. Phys. G* **35**, 063101 (2008).
- I. Sick, *Lect. Notes Phys.* **745**, 57 (2008).
- D. Shiner, R. Dixon, V. Vedantham, *Phys. Rev. Lett.* **74**, 3553 (1995).
- E. Eyler *et al.*, *Eur. Phys. J. D* **48**, 43 (2008).

Acknowledgments: This work, as part of the European Science Foundation EuroQUAM Programme, was financially supported by the Dutch Foundation for Fundamental Research on Matter (FOM). J.S. acknowledges financial support from the EC's Seventh Framework Programme (LASERLAB-EUROPE). M.D.H. and K.S.E.E acknowledge financial support from the Netherlands Organization for Scientific Research (NWO). We would like to thank J. Bouma for technical support, and J. C. J. Koelmeij and K. A. H. van Leeuwen for fruitful discussions. We also thank G. W. F. Drake, K. Pachucki, and V. A. Yerokhin for sharing the calculated theoretical parameters detailed in SOM.

Supporting Online Material

www.sciencemag.org/cgi/content/full/333/6039/196/DC1
Materials and Methods
SOM Text
Figs. S1 and S2
Table S1
Reference (32)

4 March 2011; accepted 16 May 2011
10.1126/science.1205163